Energy-dependent dead-time correction in digital pulse processors applied to silicon drift detector's X-ray spectra

Suelen F. Barros,* Vito R. Vanin, Alexandre A. Malafronte, Nora L. Maidana and Marcos N. Martins

Instituto de Física, Universidade de São Paulo, Rua do Matão 1371, Cidade Universitária, CEP 05508-090, São Paulo, SP, Brazil. *Correspondence e-mail: suelenb@if.usp.br

Dead-time effects in X-ray spectra taken with a digital pulse processor and a silicon drift detector were investigated when the number of events at the low-energy end of the spectrum was more than half of the total, at counting rates up to 56 kHz. It was found that dead-time losses in the spectra are energy dependent and an analytical correction for this effect, which takes into account pulse pile-up, is proposed. This and the usual models have been applied to experimental measurements, evaluating the dead-time fraction either from the calculations or using the value given by the detector acquisition system. The energy-dependent dead-time model proposed fits accurately the experimental energy spectra in the range of counting rates explored in this work. A selection chart of the simplest mathematical model able to correct the pulse-height distribution according to counting rate and energy spectrum characteristics is included.

1. Introduction

In most detection systems there is a minimum time interval between two pulses that allows for their identification as separated events, which is associated with the time required to record one count and called *dead-time* (Knoll, 2010; Jenkins *et al.*, 1995). Two pulses with overlapping dead-times generate a single deformed pulse (pile up), which may give rise to a count in the observed spectrum, but that does not fall in either of the positions expected for the isolated pulses; hence, both pulses are effectively lost, and one unwanted event is recorded whenever the system cannot veto its acquisition. When working at high counting-rates, the effects of dead-time and pile-up are blended and introduce important distortions in the energy spectrum, requiring a model for their correction (Lindstrom & Fleming, 1995).

Counting rates of magnitude of 10^5 Hz in X-ray spectroscopy are achievable with silicon drift detectors (SDDs) (Gatti & Rehak, 1984), which have good efficiency (Scholze & Procop, 2001; Barros *et al.*, 2017) and high resolution. For these reasons, they have become the choice for most energy-dispersive X-ray spectroscopy (EDS) measurements. This work deals with the procedures for correcting the distortions caused by dead-time and pile-up in X-ray spectra taken at high counting rates with one of these detectors using a digital pulse processor (DPP).

The approach taken here for the model development follows the classical lines detailed by Knoll (2010) and Jenkins *et al.* (1995) and accounts for specificities of this type of spectrometer (Redus *et al.*, 2008; Woicik *et al.*, 2010; Walko *et*

Energy (keV)
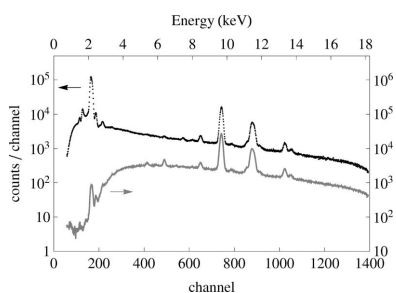
al., 2008; Ciatto *et al.*, 2004). These authors, however, dealt mostly with experimental arrangements that worked with low counting rates in the low-energy part of the spectrum and neglected the pile-up effect, which is relevant when the counting rate is high. Furthermore, it was noticed by Redus *et al.* (2008), and verified in our work, that the dead-time tends to vary in the low-energy region of the spectrum, implying that standard models are not adequate when the counting rate in this region is high. This problem is of interest in studies that involve characteristic X-rays below or around 3 keV, where dead-time variations may be important. The spectrum of Au excited by 18.5 keV electrons, shown in Fig. 1, serves as an example, with its *M* X-rays around 2.1 keV. One of the spectra shown has less than 2% of the counts under 3 keV, while the other has more than 50%. In this last spectrum, the usual dead-time correction methods proved to be inaccurate.

We propose an analytical model that allows accurate correction of the counting losses due to dead-time. It was tested under two different conditions: when the counting rate in the low-energy end of the spectrum is a large fraction of the total, and when that counting rate is much smaller than the total rate. In the experiment, described concisely in §2 and in detail in the supporting information, the photon source was provided by an electron beam hitting an Au target, yielding X-ray spectra of constant shape at rates that can be varied with the beam current. We found that the dead-time changes quickly with energy in the low-energy region, as shown in Fig. 2, where the ratio between a spectrum taken at a given counting rate and a spectrum taken at about 1 kHz is shown for several counting rates. Note that the spectra are not affected uniformly, with losses below 3 keV being more intense than at higher energies, particularly at higher counting rates. This figure also illustrates that dead-time losses at counting rates of tens of kiloHertz are a zeroth-order effect and cannot be neglected.
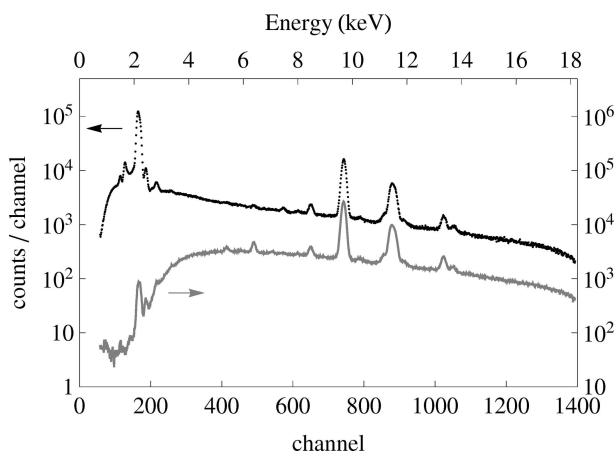

Figure 1
X-ray energy spectrum from the impact of 18.5 keV electrons at 4 kHz input rate. The dispersion in energy is 13 eV per channel. The spectrum plotted in the dotted line (black) has more than half of the counts below 3 keV. The spectrum in the continuous line (gray) was taken with an attenuator, and less than 2% of the counts fall below 3 keV. These spectral shapes will be referred to as *ML* and *L*, respectively, after the dominating Au X-ray lines.
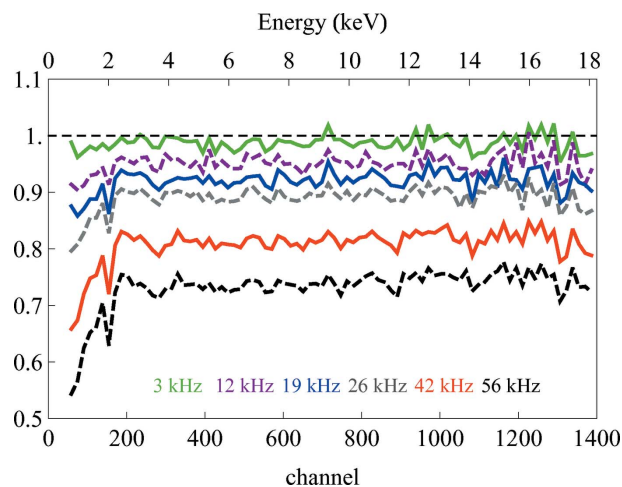

Figure 2
From top to bottom the plots represent the Au spectra acquired at rates of 3, 12, 19, 26, 42 and 56 kHz, normalized for charge and divided by the spectrum acquired at 1 kHz. Compressed spectra, dispersion 210 eV bin^{-1}.

The equations developed in §3 allow the dead-time dependence on energy to be accounted for and are based on the works of Jenkins *et al.* (1995) and Redus *et al.* (2008). §4 groups these formulas in a bunch of different models with varying degrees of accuracy (and complexity), assigning acronyms for reference in the next sections. Results obtained with the different models are presented and discussed in §5, along with a table that lists the simplest models that can provide the demanded accuracy for a given experiment, according to count rate and spectral shape. The supporting information provided with this paper contains a detailed account of the experiment and other application examples. The closing remarks are in the *Conclusion*. A list of the symbols used throughout the text is given in Appendix *A*.

2. Experiment

2.1. Experimental arrangement and procedure

The photon source consisted of the X-ray spectra produced by 18.5 keV electrons hitting a thin Au film. The São Paulo Microtron electron accelerator (Instituto de Física, Universidade de São Paulo, Brazil) beamline and vacuum chamber described elsewhere (Vanin *et al.*, 2017; Fernández-Varea *et al.*, 2014; Barros *et al.*, 2015) were employed.

The emitted photons were detected by a SDD with a DPP. The SDD has a Si crystal of 0.5 mm thickness and 2.8 mm in diameter, a 12.7 μm-thick Be window and a internal collimator of diameter 4.65 mm, made by Amptek (Bedford, USA). The detector was placed under vacuum in the irradiation chamber, and a magnet deflected the electrons scattered in the target before reaching the detector.

The digital spectrometer peaking time and the flat top of the slow channel were maintained at 1.6 μs and 0.2 μs, respectively, assuring energy resolution better than 170 eV at the Au $L\alpha_1$ (9.71 keV) X-ray line in all spectra. The peaking time of the fast channel was fixed at 100 ns.

Low-energy X-rays from the irradiated target were attenuated by a 25 μm-thick kapton film placed in front of the detector beryllium window to obtain the spectra with few counts near the energy threshold. The beam current was varied from 10 to 700 nA to take spectra with counting rates in the range 1–56 kHz. Fig. 1 shows spectra obtained at 4 kHz for both experimental conditions studied. The total charge incident on the target was measured in coincidence with the multichannel analyser enable signal, and hence it is proportional to the true input count rate.

2.2. Pile-up and dead-time in the spectrometer operation

The DPP has a single analog-to-digital converter (ADC), and two signal processing channels, named 'slow' and 'fast'. With PUR (pile up rejection) turned on, the slow channel will register a pulse if its peak amplitude is above the slow-threshold setting and below full-scale, and the fast channel does not detect two pulses within the conversion time of the slow channel.

The acquisition system records quantities which can be used to deduce the dead-time: the total numbers of counts above the thresholds in the fast and slow signal processing channels, i.e. N_{fast} and N_{slow}, respectively; and the spectrum acquisition time interval, T_{acq}, which is the multichannel analyser enabled time, and is therefore smaller than the elapsed time. Neglecting pile-up both in the fast and in the slow channels, the ratio of dead-time, T_{d}, to acquisition time is given by

$$\frac{T_{\text{d}}}{T_{\text{acq}}} \simeq \frac{N_{\text{fast}} - N_{\text{slow}}}{N_{\text{fast}}}, \tag{1}$$

which is reported to the DPP user by the acquisition system as the dead-time fraction (Amptek A, undated), and provides an estimate of the fractional loss of counts due to dead-time effects.

3. Quantifying losses from dead-time and pile-up

Good reviews on the extensive literature are given by Knoll (2010) and Jenkins et al. (1995). The model developed here derives from the works of Jenkins et al. (1995) and Redus et al. (2008), who have already noticed that the dead-time tends to vary with energy in the low-energy region of the spectrum, and was adapted to the specificities of X-ray energy-dispersive spectroscopy with DPPs. Many of the details in this section, particularly in §3.4 and §3.5, address the determination of the model parameters from the experiment, some checks on model consistency, and the evaluation of the accuracy of the correction, which are not required when the model parameters are known. The formulas of §3.1 to §3.3 with parameters taken from DPP settings and the acquired spectrum can achieve the necessary accuracy in most cases.

3.1. Dead-time

It is habitually assumed that the relation between the true input rate, R_{in}, and the true output count rate, R_{out}, when using

a paralyzable system (Redus et al., 2008; Woicik et al., 2010), like the setup examined here, is

$$R_{\text{out}}(R_{\text{in}}; \tau_{\text{C}}) = R_{\text{in}} \exp(-R_{\text{in}}\tau_{\text{C}}), \tag{2}$$

where τ_{C} corresponds to the dead-time per pulse.

This formula requires changes to account for the increase in losses at low energies, like those shown in Fig. 2. When dead-time is energy dependent, the input and output rates will also depend on energy (Jenkins et al., 1995), then

$$R_{\text{out}}(E, R_{\text{in}}) = \mathcal{R}_{\text{in}}(E) \exp[-R_{\text{in}}\tau(E)], \tag{3}$$

where $\mathcal{R}_{\text{in}}(E)$ is the input rate of photons of energy E, R_{in} is the total input rate, summed over all photon energies, and $\tau(E)$ is the dead-time per pulse corresponding to energy E, related to the conversion time of the digitizer and its operation mode.

For the slow channel, the dead-time per pulse is a generalization of the equation given by equation (1) of Redus et al. (2008). In order to account for the PUR mode of the analyser, we define δ_{rej}, which is 0 when this mode is turned 'off', and 1 if it is 'on'. The dead-time for a pulse corresponding to energy E is

$$\tau(E; E_{\text{d}}, T_{\text{a}}) = (1 + \delta_{\text{rej}})\left(1 + \frac{E_{\text{d}}}{E}\right)T_{\text{a}}, \tag{4}$$

where the meaning of E_{d} will be explained below, and the pulse-shape time constant T_{a} is defined by characteristics of the DPP,

$$T_{\text{a}} = T_{\text{peak}} + T_{\text{flat}}, \tag{5}$$

where T_{peak} and T_{flat} are the slow channel time-to-peak and flat-top time intervals, respectively.

The term $(E_{\text{d}}/E)T_{\text{a}}$ in equation (4) accounts for the time required by the analyser to sense that the pulse peaked; hence, E_{d} is the equivalent in energy to the voltage drop in the slow-channel pulse needed to identify that it has peaked, and we will call this parameter the *pulse peak-sensing threshold*. In Redus' report (Redus et al., 2008), τ_{C} of equation (2) is written in a somewhat different notation, as

$$\tau_{\text{C}} = (1 + \delta_{\text{rej}})(1 + F)T_{\text{a}}, \tag{6}$$

where F is the average fraction of the pulse fall-time needed to sense that it has peaked. Redus et al. (2008) state that, when the pulses have equal rise and fall times, F can be estimated by the ratio of the slow discriminator setting to the average energy value in the observed spectrum; this requires setting the slow threshold just above the noise level, as described in §2.2. However, we suggest that when the fraction of events recorded in the low-energy region is not small, it is better evaluated as

$$F = E_{\text{d}}\langle 1/E \rangle, \tag{7}$$

where $\langle 1/E \rangle$ is the weighted average of $1/E$ over the spectrum.

3.2. Pile-up events distribution function

The number of pile-up events $p(\ell)$ in channel ℓ can be well approximated by (Vanin et al., 2016)

$$p(\ell) = \eta \sum_c s(\ell - c + k)\,s(c), \qquad (8)$$

where k is the channel number corresponding to null photon energy, and η is a constant parameter, related to the fast digitizer time constants, as shown below.

In order to deduce the pile-up rate in the fast channel, $R_{\text{pile,fast}}$, from the dead-time per pulse in the fast channel, τ_{fast}, we substitute τ_{fast} for τ_C in equation (2), expand the exponential keeping only the first-order term, and rearrange the resulting equation, obtaining

$$R_{\text{pile,fast}} = R_{\text{in}} - R_{\text{out,fast}} = R_{\text{in}}^2 \tau_{\text{fast}}, \qquad (9)$$

where the first identity is valid only when pile-up is not rejected, as in the fast channel. This rate can be related to the pile-up distribution in the slow channel by

$$R_{\text{pile,fast}} = \frac{\sum_\ell p(\ell)}{T_{\text{acq}}} = \eta\,\frac{N_{\text{slow}}^2}{T_{\text{acq}}}. \qquad (10)$$

The deduction of this last identity requires summing the distribution given in equation (8).

From equations (9) and (10) and using $R_{\text{in}} = N_{\text{fast}}/T_{\text{acq}}$, the parameter η can be related to DPP settings,

$$\eta = \left(\frac{N_{\text{fast}}}{N_{\text{slow}}}\right)^2 \frac{\tau_{\text{fast}}}{T_{\text{acq}}}, \qquad (11)$$

wherein τ_{fast} can be evaluated from the DPP settings, using equation (6) with $\delta_{\text{rej}} = 0$.

The equations given above assume that the pile-up rate is relatively small, because $s(\ell)$ includes the effects of pile-up. In the present case, accounting for pile-up in $\mathbf{s}$, $\mathbf{s} = [s(\ell), \ell =$ channel number], in equation (8) represents a second-order correction that was neglected. Also, equation (8) does not account for triple pile-up, which is a small fraction of the counts even at counting rates of 50 kHz, the exception being strong transitions whose triple pile-ups would peak in a region where the continuum component of the spectrum is small. This is also not the case in the experiment performed, *i.e.* the triple pile-ups of M X-rays fall in a region where they cannot stand out of the continuum, hence they were neglected.

3.3. Net and compensated spectra

When a pile-up event is recorded in the spectrum the distribution of these losses is given by

$$p_{\text{loss}}(\ell) = 2\eta N_{\text{slow}}\,s(\ell), \qquad (12)$$

where $N_{\text{slow}} = \sum_k s(k)$ is the total number of counts observed in the spectrum. The factor of 2 comes from the fact that two counts were lost in the measured spectrum for each count recorded in the pile-up distribution of equation (8).

Correcting the observed spectrum for pile-up requires the subtraction of pile-up events and the replacement of the events that piled-up. Accordingly, the equation

$$n(\ell) = s(\ell) - p(\ell) + p_{\text{loss}}(\ell) \qquad (13)$$

gives a better approximation that we will refer to as the *net spectrum*. Using equation (3) to compensate for dead-time

losses, we arrive at the best approximation for the input event distribution, which we call the *compensated spectrum*,

$$S(\ell) = n(\ell) \exp\!\big[R_{\text{in}}\tau(\ell)\big], \qquad (14)$$

with $\tau(\ell) = \tau[E(\ell)]$.

3.4. Evaluation of the total output rate

The *observed* counting rate is usually evaluated as

$$\tilde{R}_{\text{out}} \simeq N_{\text{slow}}\big/T_{\text{acq}}, \qquad (15)$$

with N_{slow} and T_{acq} defined in §2.2. However, the spectrum acquired through the slow channel contains pile-up events that were not rejected because they piled up in the *fast* channel; this effect was taken into account when the net spectrum was evaluated in §3.3, and here we show the corresponding correction in the total output rate. When pile-up went undetected, two photons entered the detector but were recorded as one. Thus, the *corrected* counting rate can be estimated with

$$\hat{R}_{\text{out}} \simeq \tilde{R}_{\text{out}} + R_{\text{pile,fast}}. \qquad (16)$$

This relation can be obtained also from the ratio between the total number of counts in the net spectrum given by equation (13) and T_{acq}.

3.5. External evaluation of the input rate

In this experiment, the X-rays were produced by electron impact on a particular target, therefore the rate R_{in} is directly proportional to the beam current (Woicik *et al.*, 2010), and the *shape* of the input spectra, $\mathcal{R}_{\text{in}}(E)$, is independent of the current. Since the experimental quantities observed are the charge collected during the spectrum measurement, C, and the spectrum acquisition time, T_{acq}, the total input rate is

$$R_{\text{in}} = R_{\text{in}}\big(C, T_{\text{acq}}; P\big) = P\,\frac{C}{T_{\text{acq}}} = PI_{\text{beam}}, \qquad (17)$$

where P is a constant to be determined from the observed spectra. Many graphs in §5 will display quantities as functions of I_{beam}, since it is directly proportional to the input rate R_{in} and is not affected by photon detection effects. When a run at low counting rate can be made, and the number of events counted in the fast channel, $N_{\text{fast,LR}}$, is available, a very good approximation for P is

$$\hat{P} = N_{\text{fast,LR}}\big/C_{\text{LR}}, \qquad (18)$$

where C_{LR} is the collected charge at low-counting rate. A possible although not recommended alternative to $N_{\text{fast,LR}}$ in this formula is the total number of counts in a spectrum taken at a very low rate.

The relation between the *observed* counting rate $\tilde{R}$, equation (15), and the true input rate is obtained substituting $\hat{R}_{\text{out}}$ and R_{in} of equations (16) and (17) for the respective quantities in equation (2), which gives

$$\tilde{R}_{\text{out}}(C, T_{\text{acq}}; P, \tau_C) = P \frac{C}{T_{\text{acq}}} \exp\left(-P \frac{C}{T_{\text{acq}}} \tau_C\right) - R_{\text{pile,fast}},$$

(19)

with τ_C given by equation (6).

4. Data analysis

The procedures for compensation of dead-time losses that will be used in the subsequent sections are presented here. Whenever the dead-time per pulse can be considered energy independent, the concept of dead-time fraction can be used to correct for the losses. The compensated spectrum is then estimated by

$$\mathbf{S} = \frac{\mathbf{n}}{1 - \varphi},$$

(20)

where the *fractional loss*, φ, depends on the adopted dead-time loss model, and will be given below.

4.1. The standard model (SM)

The first-order correction for dead-time losses consists of adopting equation (2) with the output rate R_{out} given by equation (15), therefore neglecting pile-up in the fast channel. The simplest version uses the dead-time per pulse, τ_C, calculated using formula (6) with the digitizer time constants taken from DPP settings; this is the standard model with manufacturer parameters, SM_0. Notice that R_{in} in SM_0 is the solution of equation (2) using $R_{\text{out}} = [\sum_\ell s(\ell)]/T_{\text{acq}}$, which is a simple numerical procedure, described in connection with the energy-dependent model, in §4.3.1.

When spectra at different acquisition rates are obtained, it is possible to fit τ_C of expression (2) to the experimental data by a least-squares procedure, where R_{in} is estimated from P according to equation (17), hence the fitting parameters are τ_C and P. This is the standard model with fitted parameters, SM_f.

In the scope of the SM, the concept of measurement dead-time is meaningful, and the fraction of lost events is the ratio between dead-time and acquisition time, that can be evaluated by equation (1). Therefore, the fractional loss is predicted as a function of the input rate by

$$\varphi = 1 - \exp(-R_{\text{in}} \tau_C).$$

(21)

4.2. The standard model with pile-up correction (SMP)

This correction model is characterized by replacing the raw spectrum with the net spectrum $\mathbf{n}$ given by formula (13). The corrected output is the compensated spectrum of equation (14).

The simplest approach is to determine τ_C and τ_{fast} from DPP settings, and adopt formula (11) to evaluate η, required for the pile-up distribution that went undetected in the fast channel; we call it SMP_0.

A procedure that allows the accuracy of the values extracted from DPP settings to be checked is to fit the para-

meters to the spectra taken at different rates. First, the parameter η of the pile-up distribution given by equation (8) is fitted to a region of the experimental spectrum dominated by pile-up events, and then both P and τ_C of equation (19) are fitted to all available data in a single step, which is performed by a linear least-squares procedure isolating the term

$$P \frac{C}{T_{\text{acq}}} \exp\left(-P \frac{C}{T_{\text{acq}}} \tau_C\right)$$

and taking logarithms of both sides of the resulting equation. We named this procedure SMP_f.

In this case, the concept of measurement dead-time is meaningful only if pile-up effects are taken into account, hence equation (1) cannot be used directly. The best estimate is given by equation (21) with R_{in} from relation (17) and adopting the fitted values of τ_C and P.

4.3. The energy-dependent model with pile-up correction (EDP)

This model relates output and input rates by equation (3) with the energy-dependent dead-time per pulse, $\tau(E)$, given by equation (4). It requires one additional parameter, the pulse peak-sensing threshold, E_d. In the EDP model, the concept of acquisition dead-time is not useful, since the correction factor depends on the photon energy. It is the compensated distribution of equation (14) that should be used to estimate the photon spectrum.

In the next item, we show how to correct the spectra when all parameters are known, then we describe separately two different approaches to determine their values from experimental spectra taken at different counting rates.

4.3.1. Routine method. The EDP model with known E_d and T_a, equation (4), can be solved for R_{in}. The continuous line in the plot of Fig. 3 shows the quantity
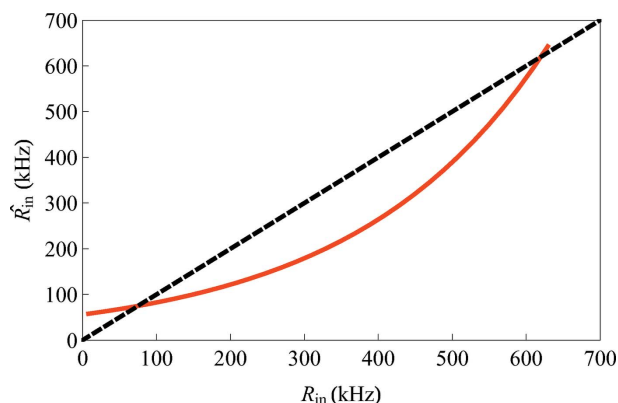
$$\hat{R}_{\text{in}} = \sum_\ell S(\ell)$$

(22)

Figure 3
The continuous line shows the quantity $\hat{R}_{\text{in}}$ of equation (22), when the compensated spectra $S(\ell)$ are evaluated for R_{in} (in the abscissa) using formula (14), for the run without X-ray attenuator at 56 kHz. Its intersection with the dashed line representing $\hat{R}_{\text{in}} = R_{\text{in}}$ that is nearest to the origin is the solution of equation (22).

evaluated from $S(\ell)$ of equation (14), with the fitted values of E_d and T_a, as a function of R_{in} (like most fitting procedures, we forget for a while that this quantity has a 'true' value), for a large range of R_{in}, in order to explain the numerical procedure. The dashed line is just the line $\hat{R}_{in} = R_{in}$; therefore the intersection nearer to the origin is the R_{in} sought, and the other intersection is a spurious solution. This procedure, using E_d and T_a from the DPP settings, corresponds to the EDP$_0$ model. The same one works with SM$_0$: once τ_C is known, the input rate R_{in} can be determined from the observed output rate by solving the non-linear equation (2). The plot of $R_{out} \exp(R_{in}\tau_C)$ versus R_{in} in SM$_0$ is very similar to that of Fig. 3.

4.3.2. Low rate spectrum as reference. In this approach, each net spectrum is normalized by the corresponding incident charge and divided by the reference spectrum, also normalized by the respective charge. This reduced spectrum at rate $R_{in,i}$, where the integer index i numbers the irradiation runs, $1 \le i \le m$, is given by

$$z_i(E) = \frac{n_i(E)}{n_{LR}(E)} \frac{C_{LR}}{C_i} \qquad (23)$$

and corresponds to the ratio $R_{out}(E)/\mathcal{R}_{in}(E)$ of equation (3). Therefore the parameters E_d and T_a of the function $\exp[-R_{in,0}\tau(E; E_d, T_a)]$ with $\tau(E; E_d, T_a)$ given by equation (4) can be fitted simultaneously to all reduced spectra $z_i(E)$, $2 \le i \le m$, adopting the reference spectrum as $n_{LR}(E) = n_1(E)$. The model function can be linearized taking its logarithm, and its parameters are fitted to the data by a linear least-squares procedure. This is EDP$_i$, fitting individual spectra.

4.3.3. Fitting the reference spectrum. In the experiment described in §2.1 the shape of the energy spectrum is proportional to $\mathcal{R}_{in}[E(\ell)]$; therefore it is independent of the counting rate, and a common shape $v(\ell)$ can be fitted to all observed spectra. To this end, equation (3) is rewritten

$$n_i(\ell) = C_i v(\ell) \exp\{-R_{in}\tau[E(\ell); E_d, T_a]\}. \qquad (24)$$

Taking logarithms of both sides, $\ln n_i(\ell)$ becomes a linear function on

$$\boldsymbol{a} = \left(\{\ln v(\ell), \ell = 1, \ldots, N\}, E_d T_a, T_a\right),$$

where the compact notation $\boldsymbol{a}$ for the set of parameters was introduced for the sake of convenience in the next formulas and N is the number of channels in the region of interest; notice that E_d does not appear isolated but in the product $E_d T_a$, in a way similar to τ_C in the SM. Despite the large number of adjustable values, it is a robust procedure. This is the model EDP$_g$, from the global fit of the data.

The least-squares procedure requires the minimization of the merit function (Eadie *et al.*, 1971)

$$Q(\boldsymbol{a}; \mathbf{y}) = (\mathbf{y} - \mathbf{X}\boldsymbol{a})^t \mathbf{V}^{-1}(\mathbf{y} - \mathbf{X}\boldsymbol{a}), \qquad (25)$$

where the superscript t means transposition. The elements of the vector $\mathbf{y}$ are the logarithms of the spectral data normalized by the charge of the runs at different counting rates $R_{in,i}$ arranged in a single column vector

$$y_{\ell+(i-1)N} = \ln \frac{n_i(\ell)}{C_i} \quad i = 1, \ldots, m, \quad \ell = 1, \ldots, N,$$

$\mathbf{V}$ is the corresponding variance matrix and $\mathbf{X}$ is the design matrix. This matrix is sparse and the elements that are not null are given by the bands

$$\mathbf{X}_{k+(i-1)N, k} = 1, \quad i = 1, \ldots, m, \quad k = 1, \ldots, N$$

and two columns

$$\mathbf{X}_{k+(i-1)N,N+1} = -2\frac{R_{in,i}}{E(k)}, \quad i = 1, \ldots, m, \quad k = 1, \ldots, N,$$

$$\mathbf{X}_{k+(i-1)N,N+2} = -2R_{in,i} \quad i = 1, \ldots, m, \quad k = 1, \ldots, N.$$

The covariance matrix of the estimated parameters is

$$\mathbf{V}(\boldsymbol{a}) = \left(\mathbf{X}^t \mathbf{V}^{-1}\mathbf{X}\right)^{-1}. \qquad (26)$$

5. Results and discussion

All available spectra were included in the parameter fitting procedures of the adopted models. Some of the runs are used as examples here, other can be found in the supporting information.

The two experimental conditions used here, which lead to a number of counts in the low-energy end of the spectrum that is a large (>50%) or small (<2%) fraction of the total, are named '*ML*' and '*L*', respectively, after the Au X-ray lines that dominate the spectra of Fig. 1, even though the differences in dead-time are due to the fraction of events at low energy, independent of the discrete or continuous character of the photon energy distribution.

We will discuss first simpler models and then EDP to assess quantitatively this improvement and find the experimental conditions that demand its application. After this evaluation, we point out the possible causes of the remaining discrepancies between experiment and EDP, followed by a discussion on the precision of the methods, which includes a table that allows selection of the simplest model to achieve a specified accuracy according to the experimental conditions.

5.1. Performance of the standard model

The parameters P and τ_C were fitted to the experimental data in the framework of SMP$_f$ of §4.2. The plots in Fig. 4 are the output rates evaluated with these values as a function of the electron beam current, in experiments with and without the X-ray attenuator. The apparent agreement between experimental data and calculated values proves that SMP$_f$ can estimate the total output rate precisely. However, it does not mean that the spectral shape is corrected properly, as Fig. 5 shows, where *ML* and *L* spectra corrected according to SMP$_f$ are plotted as z-distributions. This model adjusts the *L* spectra reasonably, as well as the *ML* spectra at counting rates below 20 kHz, but the energy spectra are strongly distorted in the low-energy region and a slight slope of the lines that represent

the corrected spectra from 3 to 18 keV can be observed. It is worth mentioning that similar results are found when P is estimated from equation (18).
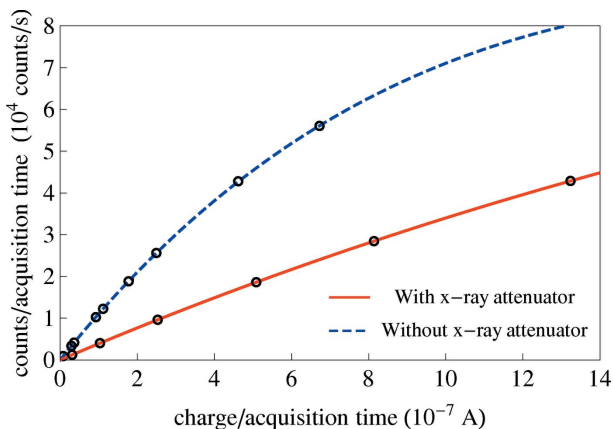

Figure 4
The points are the experimental values of R_{out} versus beam current, C/T_{acq}, for all ML and L spectra. The lines are given by SMP_f, equation (19), calculated using the parameters fitted to the ML (blue dashed line) and L (red continuous line) spectra.
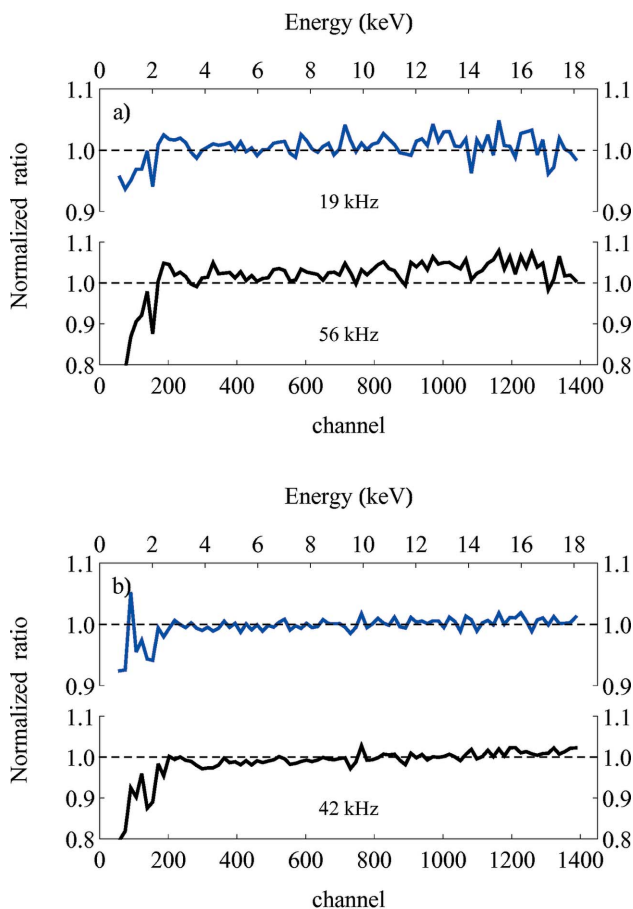

Figure 5
Ratio of a few spectra normalized by the incident charge and corrected for dead-time losses in the SMP_f framework, to the spectrum acquired at the lowest rate, also normalized by the charge, equation (23). The spectra were compressed, and each bin corresponds to 210 eV. (*a*) ML spectra and (*b*) L spectra.

The fractional count losses were evaluated by equation (21) according to both SM_0 and SMP_f and displayed in Fig. 6 along with the fractional loss estimated as the dead-time fraction given by the DPP, equation (1). The input rate was calculated using the fitted value of P in equation (17). It can be seen that the fractional loss from the DPP information is similar to that found using the SM_0 and SMP_f models for L spectra taken at all counting rates, but not for ML spectra, where the differences are perceptible at low rates and increase with counting rate.

Fig. 7 shows the z-distributions, equation (23), of the highest-rate (56 kHz) ML spectrum corrected for dead-time using the fractional count losses given by these models. The comparison between these results shows that, at high rate,
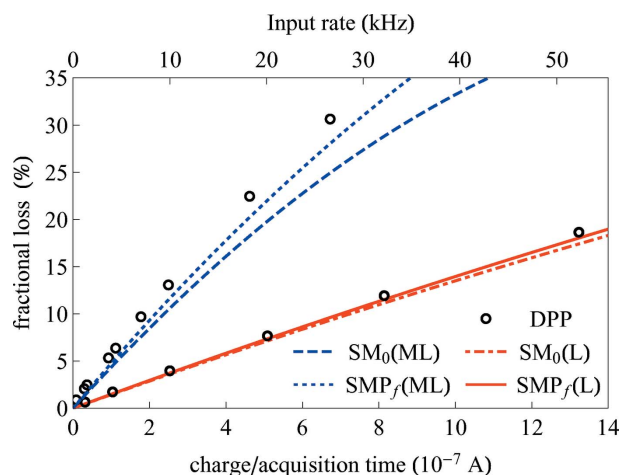

Figure 6
Estimated fractional loss of the input count rate in the ML (blue lines) and L spectra (red lines), evaluated using: the DPP information, equation (1), circles; SM_0, dotted and dot-dashed lines; and SMP_f, dashed and full lines, equation (21).
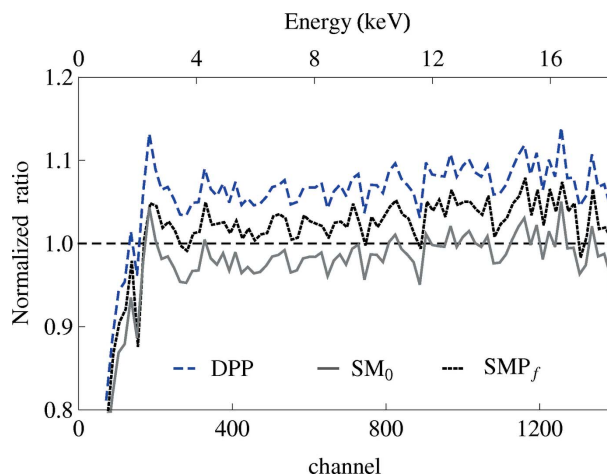

Figure 7
Ratio of the ML spectrum at 56 kHz corrected for dead-time losses to the spectrum acquired at the lowest rate, normalized by their respective charges. The dotted line (in black) was calculated with the SMP_f, the continuous line (in gray) with the SM_0 and the dashed line (in blue) with the value provided by the DPP. The spectra were compressed, and each bin corresponds to 210 eV.

Table 1
Dead-time parameters in the SMP$_f$ framework, from DPP settings using equation (6), and in the EDP model.

Columns 2 and 3 correspond to τ_C, while for EDP the shaping-time constant, T_a, and pulse peak-sensing threshold, E_d, fitted to the spectra by two different procedures are quoted. The values listed for (EDP$_i$) are the averages of the values fitted for each spectrum

Spectral shape	SMP$_f$ fit τ_C (μs)	DPP τ_C (μs)	EDP$_g$ fit T_a (μs)	EDP$_g$ fit E_d (eV)	EDP$_i$ fit $\overline{T_a}$ (μs)	EDP$_i$ fit $\overline{E_d}$ (eV)
ML	4.23 (2)	3.87	1.75 (2)	572 (26)	1.80 (2)	676 (26)
L	3.80 (1)	3.87	1.79 (3)	429 (78)	1.79 (4)	455 (26)

SMP$_f$ and SM$_0$ give more satisfactory results than using the dead-time fraction provided by DPP. SMP$_f$ compensates the underestimation in the low-energy region, responsible for half of the counts, with the overestimation of the rest of the spectrum, while SM$_0$ underestimates the correction at all energies.

The weighted averages of these z-distributions corrected for dead-time, and their respective standard deviations represented as uncertainty bars, are plotted in Fig. 8, as a function of the output count rate, for all runs and using all models, along with the same quantities obtained with the SM$_0$ and SM$_f$ models. It can be noticed that fitting τ_C in SMP$_f$ gives an effective value that improves the accuracy at high counting rate.

Table 1 gives the SMP$_f$ parameter values fitted to the experimental data, in the runs without and with the photon attenuator, compared with the respective values obtained from equation (8) using DPP settings and the energy-averaged value of the energy-dependent term, F, for all spectra. The dead-time parameters fitted to the L spectra agree with the DPP settings reasonably well, but not when fitted to the ML spectra, since a constant factor F for all photon energies cannot provide an accurate correction for every measurement condition. Additionally, the threshold of the slow channel is not a good estimate for E_d at high rates, leading to the observed differences in the τ_C parameter.

5.2. Performance of the energy-dependent model

Fig. 9 is similar to Fig. 5 described in the previous section, but corrected for dead-time losses according to the EDP$_g$ framework and replacing the reference spectrum $n_{LR}(E)$ by v in formula (23). It shows that EDP-corrected spectra present a dispersion that is much bigger below 3 keV than above it. This fuzzy behavior at low energy is assigned to distortions in the spectral shape from resolution change and peak wing growth
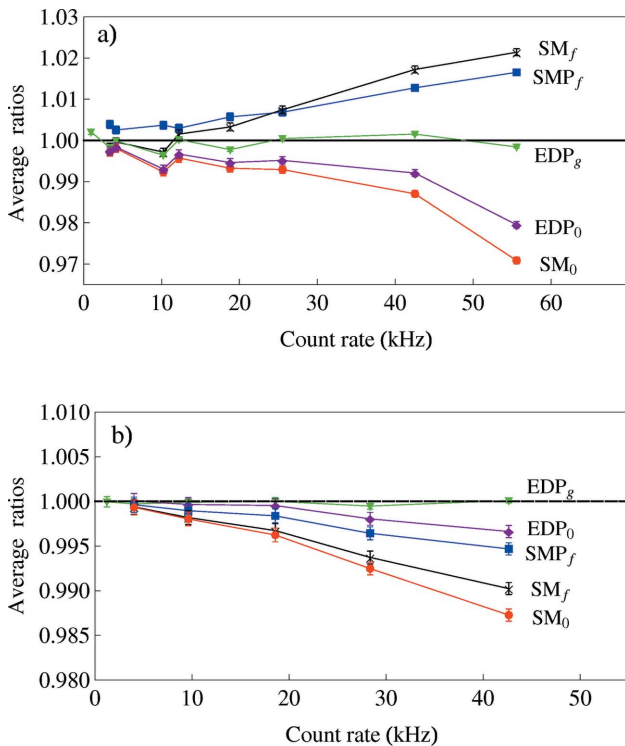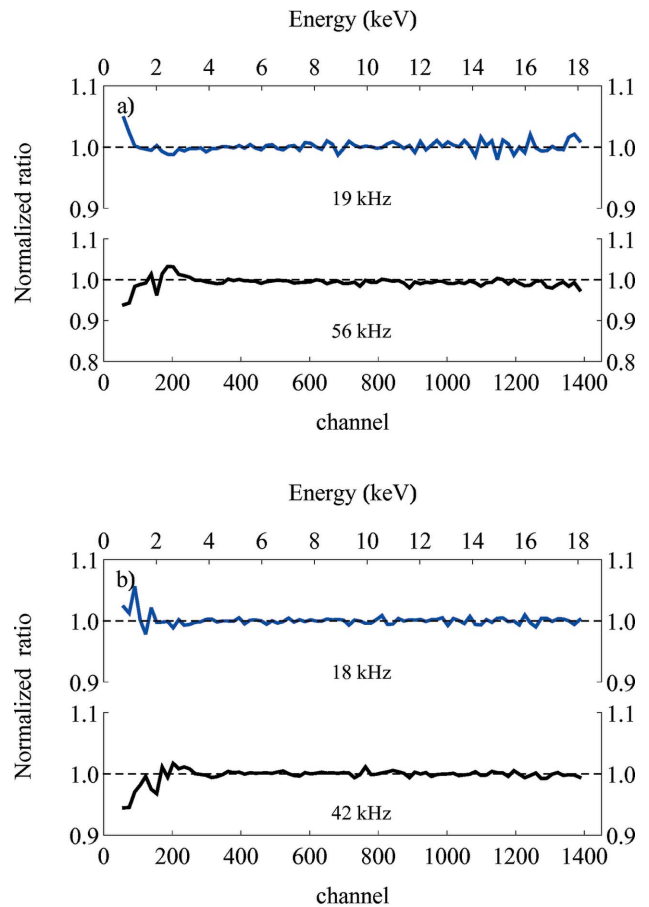

Figure 8
Weighted average of the ratio between the compensated spectrum to the reference spectrum for each run, normalized by charge, using SM$_0$, SM$_f$, SMP$_f$, EDP$_0$ and EDP$_g$ procedures, represented, respectively, by circles, crosses, squares, diamonds and triangles for (a) ML and (b) L runs.

Figure 9
Ratio of a few spectra normalized by the incident charge and corrected for dead-time losses in the EDP$_g$ framework, to the estimated reference spectrum $v(\ell)$. The spectra were compressed, and each bin corresponds to 210 eV. (a) ML spectra and (b) L spectra.

with rate, as will be discussed in §5.3. Notwithstanding this blur, the correction is adequate on average down to a few hundred electronvolts above the energy threshold. In Fig. 8 the averages of these distributions are plotted as a function of the counting rate revealing that EDP_0 gives results as accurate as those found with EDP_g at acquisition rates up to about 20 kHz. When the acquisition rate increases, the model loses accuracy, although for the L runs it remains below 0.5% even for the highest rate explored in this work, whereas for the ML runs the accuracy worsens to about 2.0% for the highest rate. Note that in this model, where T_a and E_d are fixed, there is no need for an extra experiment to estimate the input rate R_{in} (or the dead-time).

Table 1 brings the T_a and E_d values fitted to the ML and L spectra into the EDP_g and EDP_i frameworks; in the last case, the averages of the values fitted separately to each spectra are shown. The uncertainties of the values fitted by EDP_g are crude estimates, since the model does not pass a χ^2 test, owing to the significant distortions due to noise and resolution loss of the Au M X-rays. Is is found that the EDP_i and EDP_g models give compatible estimates when working with L spectra, while the agreement is only reasonable when fitted to ML spectra. Moreover, the value of T_a fitted to L spectra is compatible with that evaluated from equation (5) using the DPP settings, of 1.8 µs. Whenever fitting E_d to the individual z_i distributions, we found that its estimate is quite sensitive to the number of counts near the energy threshold. When the counting rate is low in this region, the fitted value can even be negative, in which case a reasonable procedure is to set this parameter to the energy corresponding to the maximum energy of noise events. When all the spectra are used simultaneously in the fit (§4.3.3), this problem disappears, due to the increased counting statistics.

5.3. Distortions due to pile-up and resolution loss

Fig. 10 compares the experimental ML and L spectra at the highest rate with the corresponding pile-up distributions **p** formed from the raw spectra according to equation (8), using values of η fitted to the the energy region of the spectrum situated above the bremsstrahlung tip, dominated by this effect.

The points in Fig. 11 correspond to τ_{fast}, obtained from equation (11) using the fitted values of η as a function of the input rate, R_{in}, deduced from equation (17) with the value of P fitted in SMP_f. The lines correspond to the values of τ_{fast} estimated by equation (6), with $\delta_{rej} = 0$ and F calculated according to equation (7) for both experimental situations using $T_{a,fast} = 0.1$ µs and the value chosen for the fast discriminator, $E_{d,fast} = 1.1$ keV. It is seen that the calculated values of τ_{fast} are in reasonable agreement with the value deduced from DPP settings only for L spectra. This is consistent with the adoption of an energy-independent model for pile-up in the *fast* channel and fitting the parameter η of equation (8) to the number of events above the maximum photon energy (the bremsstrahlung tip), where the pile-up events are due mostly to the Au L lines, with relatively high energies. Hence,
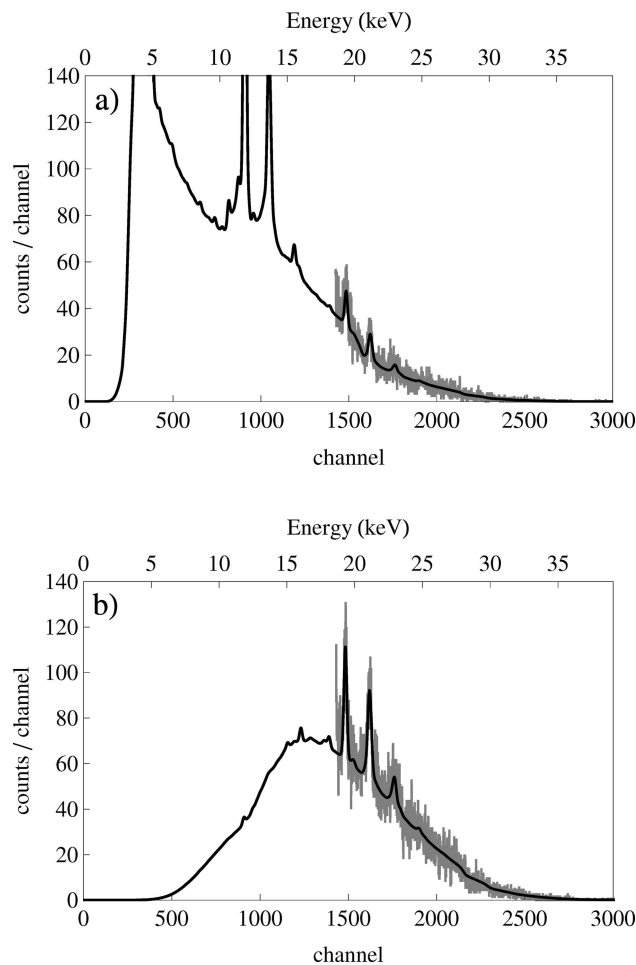

Figure 10
Experimental spectra (broken line, in gray) and pile-up model (smooth line, in black) according to equation (8), (*a*) without an X-ray attenuator at 56 kHz and (*b*) with an the X-ray attenuator at 42 kHz. The scale is chosen to highlight the pile-up events; the experimental spectrum was clipped below 19 keV. The energy dispersion is 13 eV channel^{-1}. Notice that the beam energy is 18.5 keV.
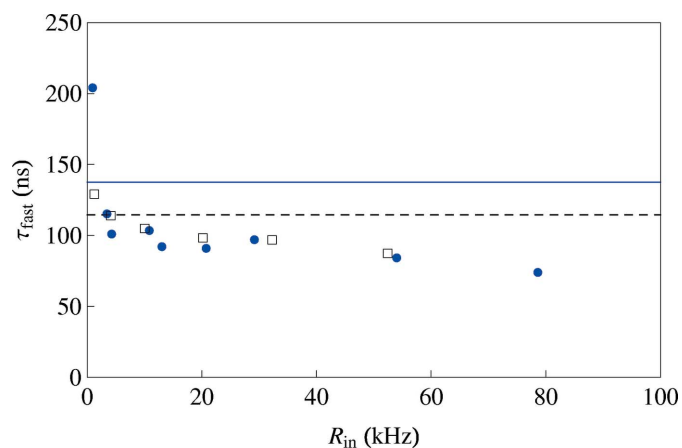

Figure 11
Estimate of dead-time per pulse associated with the fast channel, τ_{fast}. The points were determined from equations (17), (10) and (9), and the lines from equation (6). Circles and continuous line (blue) correspond to ML spectra, while squares and dashed line (black) to L spectra.

accounting for the increased dead-time at low energies is necessary and is likely the most important improvement to EDP. Two approaches seem feasible. The first one is to find the appropriate dependence on energy of the pulse pair resolution time function in the Statham model (Statham, 2006). The other is to follow the new approach given by Sabbatucci & Fernández (2017), that build a differential equation from the pulse shape. We were unable to find an explanation for the discrepancy observed with the value of τ_{fast} fitted to the ML spectrum at the lowest rate.

Ratios of ML spectra corrected by any model (examples in Figs. 5 and 9) exhibit a peak around channel 192 (at about 2.5 keV), which can be explained by resolution loss of the detector with increased acquisition rate, more severe at low energies. Note that the increased fluctuation near the threshold region in the ratios of the L spectra, Fig. 9(b), has another origin: it is caused by the small number of counts per channel in this region, which leads to important relative statistical fluctuation. However, this low counting statistic follows from the use of the attenuator, in which case this region of the spectrum is usually of no interest.

The peak shape also changes with rate due to the increase in its wings, whose proportion to the peak area rises with counting rate. Considering that this effect is more pronounced in the regions of the spectrum with high-counting-statistics peaks, which in the ML spectra were also more influenced by the loss of resolution, the dead-time correction by EDP is not able to provide results in the low-energy end as accurate as in the rest of the spectrum. Notice that resolution loss and wing formation do not affect the peak areas, although they complicate their extraction from the spectra. Therefore, the accurate measurement of the intensity of discrete photon transitions at low energies requires the EDP model for dead-time losses and accounting for the changes in peak shape with counting rate.

5.4. Precision of the corrections using the different models

The comparison between the spectra corrected by EDP_g, Fig. 9, and by SMP_f, Fig. 5, favors EDP_g, radically for ML spectra at high rates and with reduced importance at lower rates and for the L spectra. Table 2 provides a model selection key, according to counting rate, spectral shape and demanded accuracy, this last characteristic evaluated somewhat conservatively. Since dead-time scales according to the pulse-shape time constant T_a, the limits for a given precision were already reduced from this factor, meaning that the entries in the first column must be divided by T_a, in µs, to yield the rate in kHz; for example, in this experiment, where $T_a = 1.8$ µs, SM_0 should be adopted only below $30/1.8 \simeq 17$ kHz.

The accuracy of the correction provided by the different models relates to the difference between the z-distribution corrected for dead-time and unity. The average values of these differences along the complete energy spectra, plotted in Fig. 8, can be used to evaluate the improvement in the correction provided by EDP when compared with SM. The uncertainty bars reflect the dispersion of these differences, and are useful

Table 2
Model selection chart of the corrections needed to interpret the data according to the count rate.

The acquisition rate R_{out} from equation (15) was scaled for the pulse-shape time constant T_a; therefore it must be divided by the adopted T_a to find the rate in kHz.

Acquisition rate (kHz T_a/µs)	L spectra		ML spectra	
<30	SM_0	DPP	SM_0	DPP
30–60	EDP_0	DPP	EDP_0	SM_0
60–120	EDP	SM	EDP†	EDP_0†
Accuracy	0.5%†	1.0%	1.0%	2.0%

† This accuracy, however, is only achieved for the spectral region above $\sim$3 keV.

to assess the significance of the observed averages when applying the different models; in almost all cases they are sufficiently small to discriminate between the correction procedures. Note that when SM_0 and SMP_f were applied, the spectra counted at different rates were divided by the spectrum taken at the lowest counting rate, which has statistical fluctuations greater than the fitted reference spectrum, $v(\ell)$, used as normalization for the results obtained with EDP_0 and EDP_g, hence the uncertainty bars are smaller using EDP.

Since the accuracies given in Fig. 8 are averages for the whole spectrum, they do not reflect the rate-dependent deformations of the spectrum shape shown in Fig. 2. In particular, the use of a single value for correcting the number of counts in all channels of the spectrum in the SM framework underestimates the true spectrum in the low-energy end and overestimates it at the high-energy end. Therefore, the average of the z-distribution corrected for dead-time is an acceptable measurement of the accuracy only when this bias is small, hence we will adopt it as the single indicator only at low rates for SM models, while for EDP models it is unbiased and can be used at higher rates. In the case of L spectra, with few counts in the low-energy region (Fig. 9b), the statistical fluctuation of the ratio is very important, but it is difficult to be sure that the differences arise from the incompleteness of the model, as discussed in §5.3.

It should be emphasized that, although neglecting pile-up at low counting rates does not affect the overall dead-time correction, the pile-up spectrum must be evaluated, especially when weak lines are of interest, since a particular line can change much more than the general spectral shape.

Table 2 was constructed assuming that the experimenter knows the parameters necessary for the correction of the dead-time, τ_C and E_d, either because the manufacturer's manual can be trusted or they were fitted to experimental data. While the manufacturers do not provide the pulse peak-sensing threshold E_d, for the spectra at the highest rate the accuracy listed in the table can be reached only when E_d is experimentally determined and, for ML spectra, EDP_0 may not provide the listed accuracy below $\sim$3 keV. Finally, at high rates, spectra rich at the low-energy end show rate-related distortions in this region that are due to effects not taken into account by this dead-time model; therefore the accuracy listed in the table cannot be achieved in this energy region and

further studies are required to improve the quality of the correction. In the supporting information, a comparison of the shapes of the spectra corrected according to Table 2 can be examined.

6. Conclusion

We evaluated different models for dead-time counting losses in X-ray spectra taken with a DPP for two different experimental conditions, when the number of counts in the low-energy region is a small or a large fraction of the spectrum, named L and ML spectra, respectively, for input count rates up to 80 kHz. The results show that the standard model (SM), even taking into account pile-up (SMP), does not give accurate results for the ML spectra. The energy-dependent model with pile-up (EDP) proposed here corrects adequately both L and ML spectra with an average accuracy of about 0.5% and better than 1.0%, respectively.

Most of the parameters of the EDP model can be obtained from the DPP settings, but not the pulse peak-sensing threshold, E_d, which has to be fitted to spectra taken specially for this procedure. It would be welcome by the experimentalists if manufacturers include this specification in the X-ray spectrometer data sheet, avoiding this task, which requires special radiation sources, not always available in the laboratories.

Procedures easier to implement than the EDP proposed here can be adequate for the analysis in certain specific combinations of counting rates, spectral shape and required accuracy of an experiment. A selection chart of the simplest correction model for a given specification of the measurement (rate, spectral shape and accuracy) is provided in Table 2.

The energy-dependent dead-time model proposed in this paper provides an accurate correction. Nevertheless, it is still incomplete, requiring at least to take into account the energy-dependence of pile-up in the *fast* channel. Moreover, the spectral distortion at low energies, assigned to resolution loss and pile-up with noise, was not taken into account, and is required when analysing discrete spectra to achieve accurate results. We plan to undertake new experiments to investigate possible models for these effects.

7. Related literature

The following references, not cited in the main body of the paper, have been cited in the supporting information: Nascimento *et al.* (2011); Radeka (1972).

APPENDIX A
Definition of symbols

A list of the symbols used throughout the paper are given in Table 3.

Table 3
List of the symbols used throughout the text.

T_d	Dead-time
T_{acq}	Acquisition time
N_{slow}, N_{fast}	Numbers of counts above the fast and the slow threshold
R_{in}, R_{out}	True input and output rates, respectively
τ_C	Dead-time per pulse
E	Photon energy
$\mathcal{R}_{in}(E)$	True input rate of photons of energy E
$\tau(E)$	Dead-time per pulse of energy E
E_d	Pulse peak-sensing threshold
T_a	Pulse-shape time constant
F	Average time to sense that a pulse has peaked, in units of T_a
$s(\ell), p(\ell)$	Numbers of counts and pile-up events, respectively, in channel ℓ
$R_{pile,fast}$	Pile-up rate in the fast channel
$R_{out,fast}$	Output count-rate in the fast channel
τ_{fast}	Fast-channel pulse-shape time constant
η	Fraction of pile-up events per count
$S(\ell)$	Number of events in channel ℓ corrected for dead-time and pile-up
C	Charge collected, proportional to total number of counts
i, LR	One of the acquisition runs and the lowest rate run, respectively (often subscript)
I_{beam}	Electron beam current
P	Number of counts per unity charge
φ	Dead-time fraction of the acquisition time
z ratio	Of the net spectra normalized by the collected charge
$\nu(\ell)$	Number of counts in channel ℓ per unit charge

References

Amptek A (undated). *Amptek Silicon Drift Diode (SDD) at High Count Rates.* Application Note: AN-SDD-001 Rev B0, https://amptek.com/pdf/ansdd1.pdf, last accessed 15 Nov 2016. Amptek Inc.

Barros, S. F., Maidana, N. L., Fernández-Varea, J. M. & Vanin, V. R. (2017). *X-ray Spectrom.* **46**, 34–43.

Barros, S. F., Vanin, V. R., Maidana, N. L. & Fernández-Varea, J. M. (2015). *J. Phys. B*, **48**, 175201.

Ciatto, G., d'Acapito, F., Boscherini, F. & Mobilio, S. (2004). *J. Synchrotron Rad.* **11**, 278–283.

Eadie, W. T., Drijard, D., James, F. E., Roos, M. & Sadoulet, B. (1971). *Statistical Methods in Experimental Physics.* Amsterdam: North Holland.

Fernández-Varea, J. M., Jahnke, V., Maidana, N. L., Malafronte, A. A. & Vanin, V. R. (2014). *J. Phys. B*, **47**, 155201.

Gatti, E. & Rehak, P. (1984). *Nucl. Instrum. Methods Phys. Res.* **225**, 608–614.

Jenkins, R., Gould, R. W. & Gedcke, D. (1995). *Quantitative X-ray Spectrometry*, pp. 147–207. New York: Marcel Dekker.

Knoll, G. F. (2010). *Radiation Detection and Measurement*, ch. 17, 4th ed. New York: Wiley.

Lindstrom, R. M. & Fleming, R. F. (1995). *Radioact. Radiochem.* **6**, 20–27.

Nascimento, E., Fernández-Varea, J. M., Vanin, V. R. & Maidana, N. L. (2011). *AIP Conf. Proc.* **1351**, 216–220.

Radeka, V. (1972). *IEEE Trans. Nucl. Sci.* **19**, 412–428.

Redus, R. H., Huber, A. C. & Sperry, D. J. (2008). *IEEE Nucl. Sci. Conf. Rec.* pp. 3416–3420.

Sabbatucci, L. & Fernández, J. E. (2017). *Radiat. Phys. Chem.* **137**, 12–17.

Scholze, F. & Procop, M. (2001). *X-ray Spectrom.* **30**, 69–76.

Statham, P. J. (2006). *Microchim. Acta*, **155**, 289–294.

Vanin, V. R., Maidana, N. L., Mangiarotti, A., Lima, R. R., Malafronte, A. A., Barros, S. F. & Martins, M. N. (2017). *Radiat. Phys. Chem.* Submitted.

Vanin, V. R., Manso Guevara, M. V., Maidana, N. L., Martins, M. N. & Fernández-Varea, J. M. (2016). *Radiat. Phys. Chem.* **119**, 14–23.

Walko, D. A., Arms, D. A. & Landahl, E. C. (2008). *J. Synchrotron Rad.* **15**, 612–617.

Woicik, J. C., Ravel, B., Fischer, D. A. & Newburgh, W. J. (2010). *J. Synchrotron Rad.* **17**, 409–413.